Shock Waves (2002) 12: 59–68
Digital Object Identifier (DOI) 10.1007/s00193-002-0142-5

Shock Waves

Numerical study of spherical blast-wave propagation and reflection

S.M. Liang, J.S. Wang, H. Chen

Department of Aeronautics and Astronautics, National Cheng Kung University, Tainan 701, Taiwan, R.O.C

Received 27 July 2000 / Accepted 25 January 2002
Published online 17 June 2002 –

Abstract. The objective of this study is to understand the flow structures of weak and strong spherical blast waves either propagating in a free field or interacting with a flat plate. A 5th-order weighted essentially non-oscillatory scheme with a 4th-order Runge-Kutta method is employed to solve the compressible Euler/Navier-Stokes equations in a finite volume approach. The real-gas effects are taken into account when high temperature occurs. A shock-tube problem with the real-gas effect is first tested in order to verify the solver accuracy. Moreover, unsteady shock waves moving over a stationary wedge with various wedge angles, resulting in different types of shock wave reflections, are also tested. It is found that the computed results agreed well with the existing data. Second, the propagation of a weak spherical blast wave, created by rupture of a high-pressure isothermal sphere, in a free field is studied. It is found that there are three minor shock waves moving behind the main shock. Third, the problem of a strong blast wave interacting with a flat plate is investigated. The flow structures associated with single and double Mach reflections are reported in detail. It is found that there are at least three local high-pressure regions near the flat plate.

Key words: Blast wave, Real-gas effects, Regular reflection, Double Mach reflection

1 Introduction

One distinctive characteristic of a spherical blast wave is a moving shock wave accompanied by expansion waves. Due to its three-dimensional expansion the intensity of a blast wave always decays with time and distance during propagation. The flow field induced by the blast wave when interacting with a flat plate becomes more complicated because of shock wave reflection. The interaction generally includes two types of reflections: Regular Reflection and Mach Reflection. Such an interaction often occurs on our earth such as in a chemical high-explosion in factories or a nuclear weapon explosion that can destroy buildings. Many researchers are interested in the flow field induced by a blast wave and the transient dynamic loading effects when the blast wave interacts with a structure. Therefore a basic study of blast-wave propagation and interaction with a flat plate is helpful for engineering applications.

To the authors' knowledge, the papers that reported the detailed flow field induced by a strong blast wave, in particular, when interacting with a flat plate are limited because of the nonlinear decay of blast waves in its intensity. Brode (1955) numerically studied the propagation of a blast wave. The peak overpressures as a function of the shock radius were asymptotically obtained for two different initial conditions – a point source and an isothermal sphere. Later, Brode (1959) studied the blast wave propagation in a free field. The blast wave resulted from the detonation of a spherical charge of TNT. An ideal-gas assumption was made. He found that a series of subsequent minor outward-moving shocks occur behind the main shock. Dewey (1971) investigated the flow properties of a blast wave using an analysis of the particle trajectories observed by high-speed photography. However, this technique cannot be used for shocks stronger than Mach 2.5. Vanderstraeten et al. (1996) studied the blast waves generated by a bursting spherical vessel filled with a pressurized gas, and derived a simple model that is comparable to a TNT-equivalent model. They also showed that a bursting sphere could lead to more than one shock wave.

Takayama and Sekiguchi (1981) investigated the interaction problem of a spherical blast wave with a flat plate. The blast wave was generated by a planar shock wave in a shock tube moving into a free space. Their results obtained from the analysis and the experiments did not agree well. Hu and Glass (1986) theoretically analyzed the types of

Correspondence to: S.M. Liang
(e-mail: liangsm@mail.ncku.edu.tw)

blast wave reflection at different heights of burst (HOB). They found that there are two types of transition process, that is, $RR \Rightarrow SMR$ and $RR \Rightarrow DMR \Rightarrow TMR \Rightarrow SMR$, where SMR, TMR, DMR, denote single Mach reflection, transitional Mach reflection, double Mach reflection, respectively. Dewey et al. (1981) experimentally studied a blast wave interacting with a smooth surface and with a rough surface, and found that a smooth surface can induce a stronger Mach stem and a higher triple-point trajectory. Colella et al. (1986) numerically studied the flow field of a strong blast-wave interaction with a flat plate. The strong wave was obtained from the detonation of a high-explosion charge. The interaction produced a $RR \Rightarrow DMR$ transition. The numerical method they used was a second-order Gudonov scheme with a monotone property. Dixon-Hiester et al. (1989) found that there is an abrupt pressure rise in the transition region in experiments. Hisley (1990) numerically studied the reflection of planar shocks from wedge surfaces by using three computer codes – BLATST2D, SHARC and STEALTH. He found that the BLAST2D code is better than the other two codes, since the BLAST2D code produced less oscillation near discontinuities and had a better ability of capturing slip lines. The BLAST2D code is based on Roe's approximate Riemann solver with a total variation diminishing property and has second-order accuracy. Jiang et al. (1998) numerically and experimentally investigated the propagation and reflection of a micro-blast wave generated by pulsed-laser beam focusing. An initial condition of a point-source explosion was specified with the Taylor similarity law for their numerical simulation. Agreement was obtained between the numerical solution and the experimental result.

In this study, a 5th-order WENO (weighted essentially non-oscillatory) scheme of Jiang and Shu (1996) is employed for space discretization of the convective terms and central differences for the viscous terms. A 4th-order Runge-Kutta method is used for time integration. The advantage of the WENO scheme is that it is able to resolve high flow gradients and discontinuities with a tendency of avoiding the use of an adaptive grid or a very fine grid. To see the advantage and solution accuracy, our computer code was compared with the BLAST2D code. On the other hand, the present computer code is easy to use since the explicit Runge-Kutta method is used. Real gas effects are taken into account when the temperature is high by using a fitting method of Srinivasan et al. (1987) for computing the value of the specific heat ratio. To verify the accuracy of the solver developed, a shock-tube problem with real-gas effects is tested. We also tested four types of reflections of an unsteady shock wave propagating over a wedge. After the code validation, the propagation of a spherical blast wave created by the rupture of an isothermal sphere with a high pressure inside was studied. Finally a strong blast wave interacting with a flat plate was calculated to examine the transition phenomena of blast-wave reflection from a flat plate and the associated flow structure.

2 Mathematical formulation and numerical method

2.1 Governing equations

The problem of interest is the propagation and reflection of the blast wave produced by a bursting sphere with an initial pressure ratio, p_1/p_0, as shown in Fig. 1. The working fluid is assumed to be air. Assume the sphere has a radius of R_0 and is located at an altitude of HOB, the height of burst. In Cartesian coordinates, (x, y), the dimensionless governing equations are the continuity, momentum, and energy equations, which can be expressed in conservative form as

$$Q_t + \left(F - \frac{1}{Re}F_v\right)_x + \left(G - \frac{1}{Re}G_v\right)_y + \frac{\alpha}{y}\left(H - \frac{1}{Re}H_v\right) = 0 \quad (1)$$

where subscripts t, x, y denote partial derivatives and the subscript v denotes the viscous terms. The variable Q is the conservative-variable vector, F, G the inviscid-flux vectors, H the source term due to the axis symmetry, and Re the Reynolds number in which the reference velocity is chosen to be the speed of sound inside a bursting sphere and the radius (R_0) of the sphere. Moreover, F_v and G_v are the dissipation terms in the x and y directions, respectively. H_v is the dissipation term due to the axis symmetry. The expressions for F_v, G_v, and H_v can be found in the book of Hoffmann and Chiang (1993). Moreover, $\alpha = 0$ represents a two-dimensional flow, and $\alpha = 1$ for an axisymmetric flow. In order to take real-gas effects into account, a curve fitting method of Srinivasan et al. (1987) is used to determine the thermodynamic properties (such as γ) of air with the pressure and the density as two independent variables. The enthalpy, h, is computed by the relation: $h = \rho(\gamma - 1)/(\gamma p)$. Namely, the equivalent γ concept for real gas is adopted. Moreover, the fluid viscosity is computed by using a curve fitting method of Srinivasan and Tannehill (1987). For turbulent flow, a two-layer algebraic turbulent model of Baldwin and Lomax (1978) is employed.

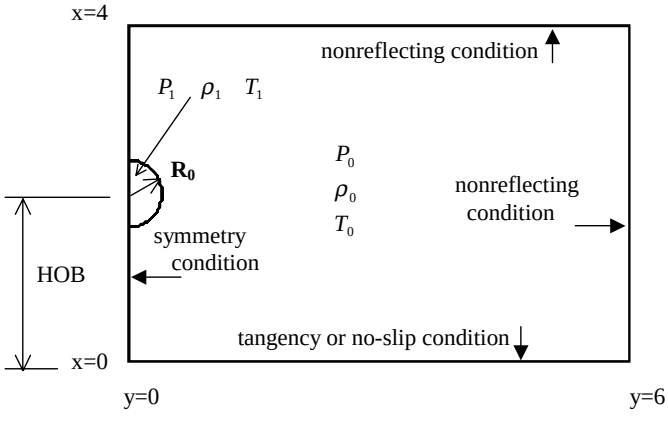

Fig. 1. A computational domain and the initial and boundary conditions

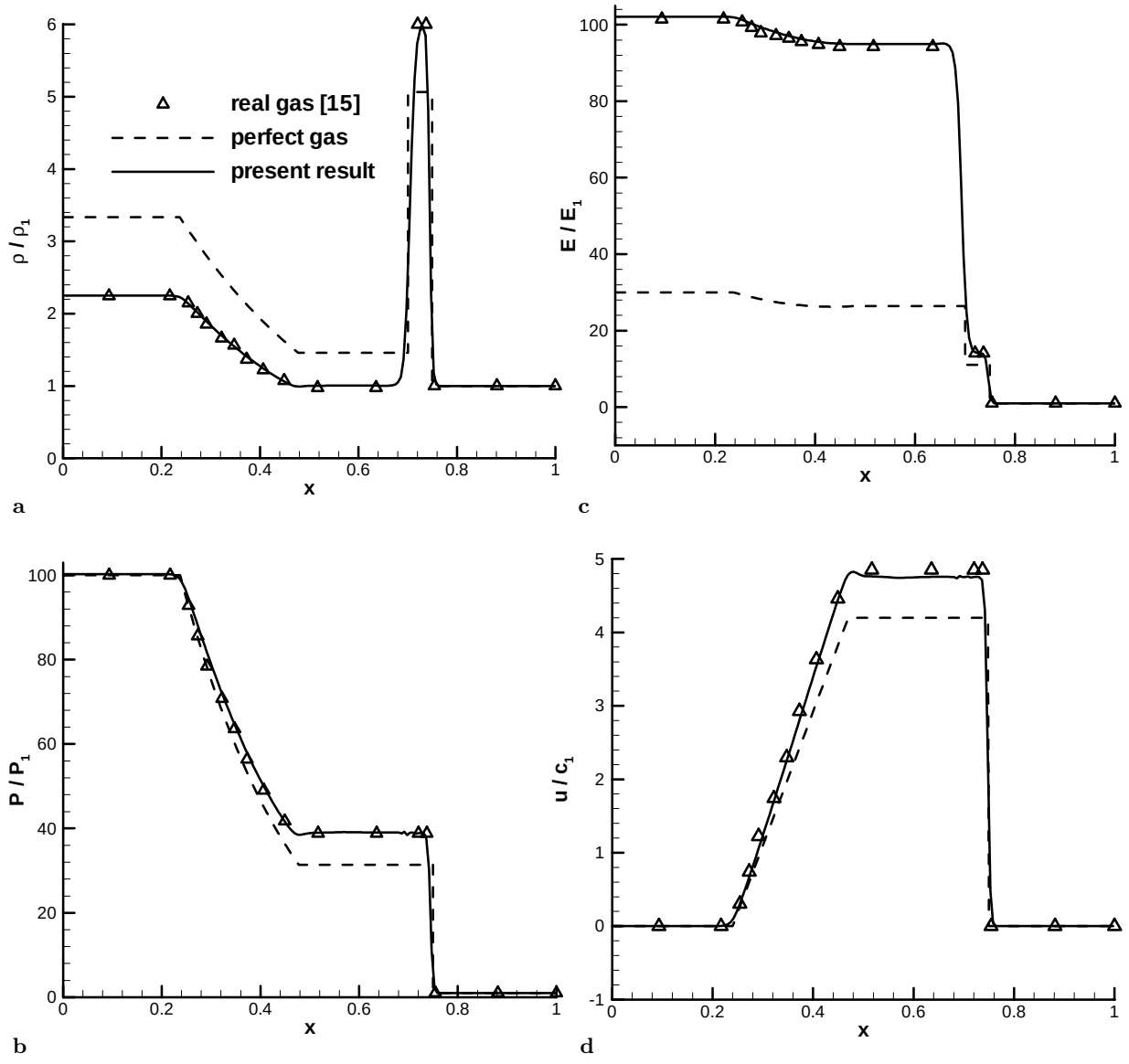

Fig. 2. The computed results of **a** the density ratio, **b** the pressure ratio, **c** the energy ratio, **d** the dimensionless velocity for a shock tube problem with the real-gas effect

2.2 Numerical method

A high-order numerical procedure of Jiang and Shu (1996) in a finite volume approach is used for solving Eq. (1). This procedure consists of a 4th-order Runge-Kutta method for time integration and a 5th-order WENO scheme for spatial discretization of the convective terms. The 2nd-order central differences are used to approximate the viscous terms. The Courant number is set to 0.6. All calculations are performed on a Pentium III-600 MHz with a 256 MB memory.

The initial state inside a bursting sphere is quiet air with a high-pressure (p_1) and high-density (ρ_1). The surrounding environment is also quiet air with $p_0 = 1\,\text{atm}$, $\rho_0 = 1.225\ \text{kg/m}^3$, $T_0 = 288.15$ K. The value of the specific heat ratio in the high-pressure region is determined from the chosen pressure and density ratios. The radius (R_0) of the bursting sphere is a geometric parameter. The boundary condition on the flat plate is the tangency condition for the inviscid-flow model and the no-slip condition for the viscous-flow model. A symmetry boundary condition is imposed at the vertical x-axis to save computation time. (Ref. to Fig. 1.) At the top and right boundaries, the nonreflecting boundary condition of Thompson (1987) is specified.

3 Results and discussion

3.1 Code validation

Case I: A shock tube problem. A shock tube problem with real-gas effects is considered. The initial states for the high-pressure side are $p_4 = 100$ atm, $\rho_4 = 2.641\text{kg/m}^3$,

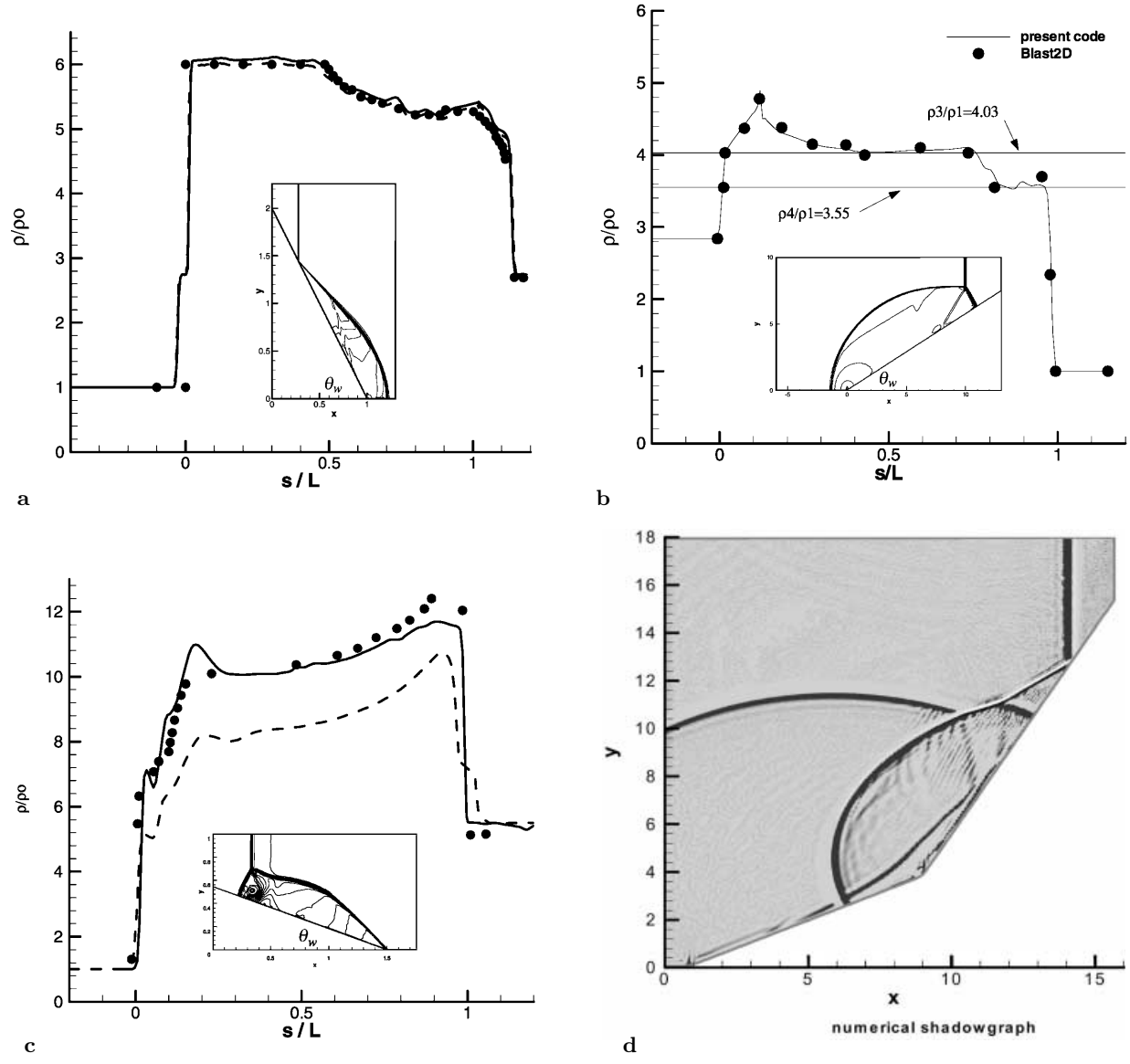

Fig. 3. The computed density distributions along the wedge surface compared with the existing data for four types of shock wave reflection, (**a**–**c**), and numerical shadowgraph, (**d**). In figures **a**–**c**, *solid line* represents real-gas model, *dash line* for perfect-gas model, *solid symbols* for the experimental data of Deschambault and Glass. In figure **b**, *solid symbols* represent Hisley's results. **a** Regular reflection, **b** single Mach reflection, **c** transitional Mach reflection, **d** inverse Mach reflection

$e_4 = 5216$ kcal/kg, $T_4 = 9000$ K, and $p_1 = 1$ atm, $\rho_1 = 1.174$ kg/m^3, $e_1 = 51.33$ kcal/kg, $T_1 = 300$ K for the low-pressure side. A uniform grid with 181×6 cells on the computed domain is $\{(x, y)|0 \le x \le 1, 0 \le y \le 0.02\}$. The diaphragm is located at $x = 0.5$. Figure 2 shows the computed pressure, density and energy ratios and the velocity distribution when the normal shock moves to the location $x = 0.75$. It is found that the present results agree well with the exact solution for real gas (Grossman and Walters, 1989). The perfect-gas result is very unsatisfactory.

Case II: Unsteady plane shock waves moving over a stationary wedge. Consider an unsteady plane shock wave moving over a wedge with the half wedge angle, θ_w. The configuration of shock wave reflection from a wedge depends upon the incident shock Mach number, M_s. Five types of reflections are tested. They are RR, SMR, TMR, DMR, and IMR, where IMR denote inverse Mach reflection. The initial conditions used are tabulated in Table 1. The computed results are shown in Fig. 3. Note that the result for the DMR case is not reported here, since the configuration of DMR is very similar to that of TMR. Figures 3a and 3c show the comparison of the computed density distributions along the wedge surface with the experimental data of Deschambault and Glass (1983). Note that the abscissa (s) denotes the distance along the wedge, and is normalized by the distance (L) from the reflection point or the Mach stem to the wedge corner. Thus the wedge corner is located at $s/L = 1$. One can see that good agree-

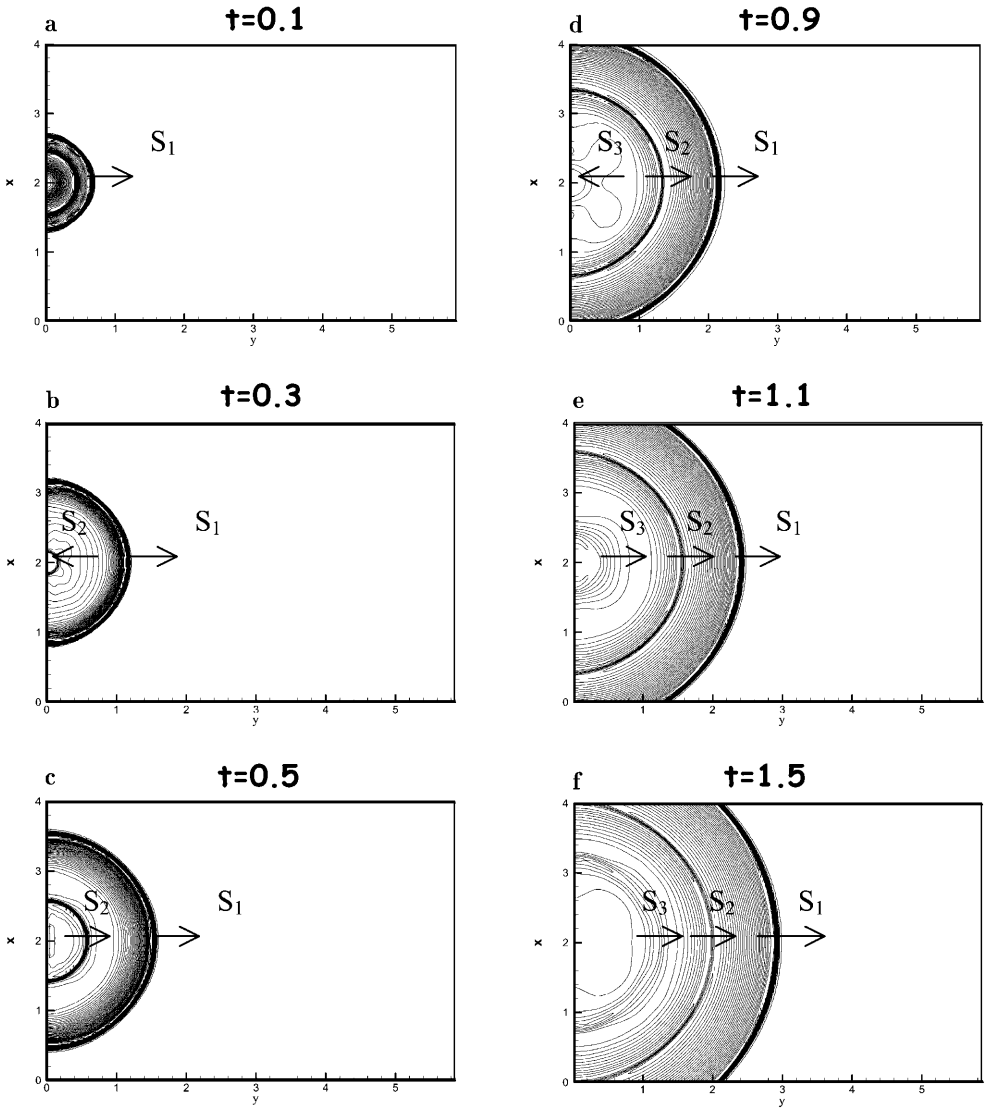

Fig. 4. Pressure contours for a bursting sphere in a free field at different instants

ment is obtained for the RR and TMR types, as shown in Figs. 3a and 3c. Figure 3b shows the comparison of the computed density distribution with Hisley's result for single Mach reflection. Obviously, good agreement is obtained too. Figure 3d shows the numerical shadowgraph for an inverse Mach reflection, which agreed very well with the experimental shadowgraph in Hisley's report (1990).

3.2 Spherical blast wave propagation in a free field

In order to understand the basic flow structure, the viscous effects of the flow are neglected. The Euler solver is used for numerical simulation. Consider an isothermal bursting sphere of pressurized air with $p_1/p_0 = 70$ and $R_0 = 0.3$. The bursting sphere is used to produce a blast wave. Three values of initial density ratio, $\rho_1/\rho_0 = 4$, 5 and 6, are chosen. It was found that these three values produce a blast wave with almost the same intensity for $r \geq 1.2$, where r denotes the radius measured from the spherical blast-wave center. Thus we choose $\rho_1/\rho_0 = 5$ for the subsequent study. The computed domain is $\{(x, y)|0 \leq x \leq 4, 0 \leq y \leq 6\}$. A 150×225 grid is used.

Table 1. The conditions used for different types of shock wave reflection over a wedge

Case	Type of shock reflection	Incident shock Mach number	Wedge angle	Number of grid
1	RR	2.05	63.4°	300×200
2	SMR	2.12	30°	189×172
3	TMR	7.19	20°	200×100
4	DMR	8.70	27°	200×100
5	IMR	1.295	25°/60°	200×200

To understand the blast-wave propagation and decay at different instants, we plotted the velocity field and temperature, density and pressure contours. Only the temperature and pressure contours are presented here. Fig-

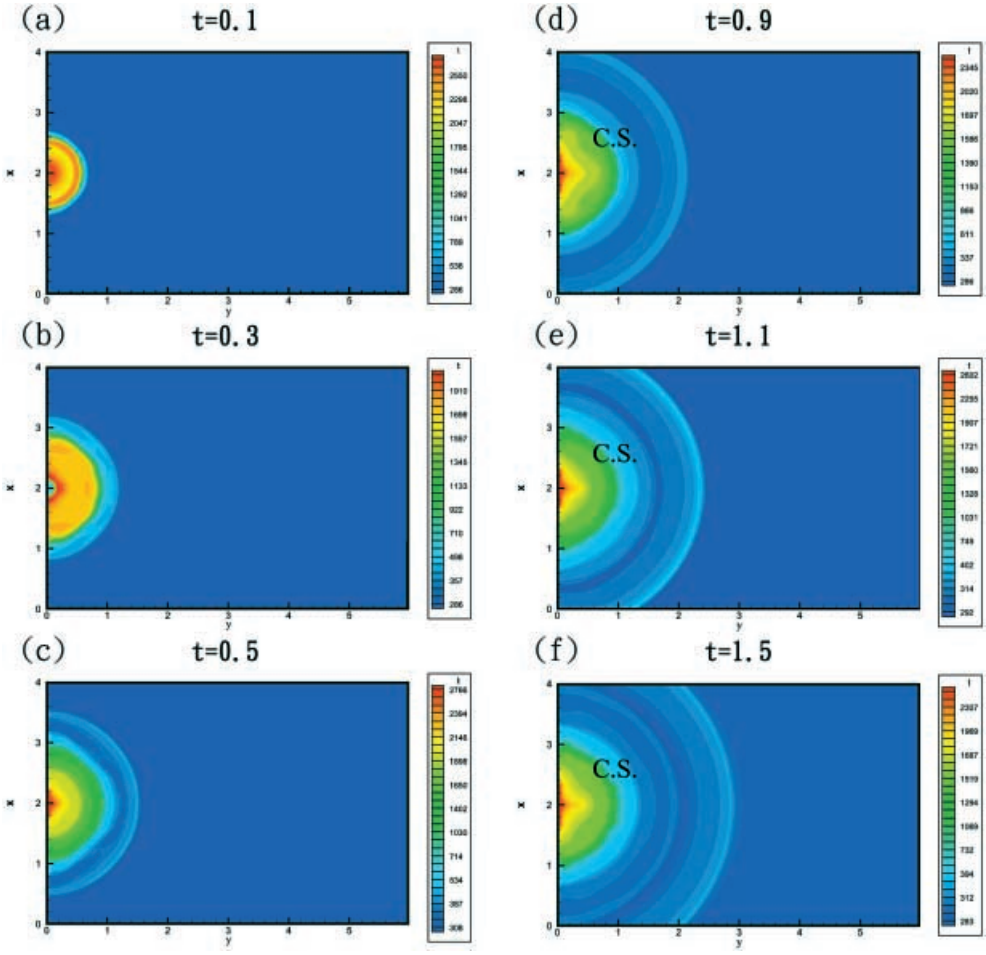

Fig. 5. Temperature contours for a bursting sphere in a free field at different instants

ure 4 shows the pressure contours at different instants. At $t = 0.1$, the primary shock wave (S_1) of the blast wave is moving outward and the expansion waves are moving inward, causing some white rings as shown in Fig. 4a. At $t = 0.3$, the effect of the expansion waves produce an inward-moving shock denoted by S_2, as shown in Fig. 4b. At $t = 0.5$, the inward-moving shock has been reflected and is moving outward, as shown in Fig. 4c. The outward-moving shock wave is referred as the secondary shock. In the time interval of $t = 0.9$–1.1, a tertiary shock wave (S_3), as shown in Figs. 4d and 4e, has developed as the secondary shock did. Figure 4f shows the three outward-moving shocks (S_1, S_2, S_3) and their accompanying expansion waves, resulting in the black and white ring-typed regions.

Figure 5 shows the temperature contours at different instants. Inside the burst sphere, the initial temperature is 2717K. At $t = 0.1$, the temperature near the burst center, a core hot region, remains the initial temperature, since the expansion waves have not reached there, as shown in Fig. 5a. At $t = 0.3$, the expansion waves have reached the core hot region, resulting in a low temperature of 620 K in a circular region with radius of 0.08. The inward-moving shock causes a temperature rise in the vicinity of the low-temperature region, as indicated by the dark-red ring in Fig. 5b. At $t = 0.5$, the temperature at the burst center reaches 2884 K, because of two passes of the inward- and out-moving shocks, S_2, as shown in Fig. 5c. For larger t, the temperature at the burst center is about 2537 K, as shown in Figs. 5d–f. A contact surface is developed at $r = 0.99$.

Figure 6 shows the pressure-time history at the selected locations with $x = HOB$ inside and outside the bursting sphere. The coordinates of these two locations are $r = 0.147$ and 0.281 for the case inside the bursting sphere, and $r = 0.9$ and 1.51 for the case outside the bursting sphere. Figure 6a depicts the pressure variations at these two points inside the bursting sphere. The solid line corresponds to the first case, and the dash line for the latter case. At the location of $r = 0.147$, the pressure remains constant for a short time until the expansion wave arrives after the burst of the sphere, as indicated by the solid line for $t = 0.1$ in the figure. After the passing of the expansion waves, the pressure rapidly drops to less than the ambient pressure, as indicated on the solid and dash lines for approximately $t = 0.2$–0.25. The under-pressure phase results in a secondary inward-moving shock wave. The inward-moving secondary shock wave causes a pressure rise for the solid line at $t = 0.27$. The inward-moving shock wave will reflect and move out-

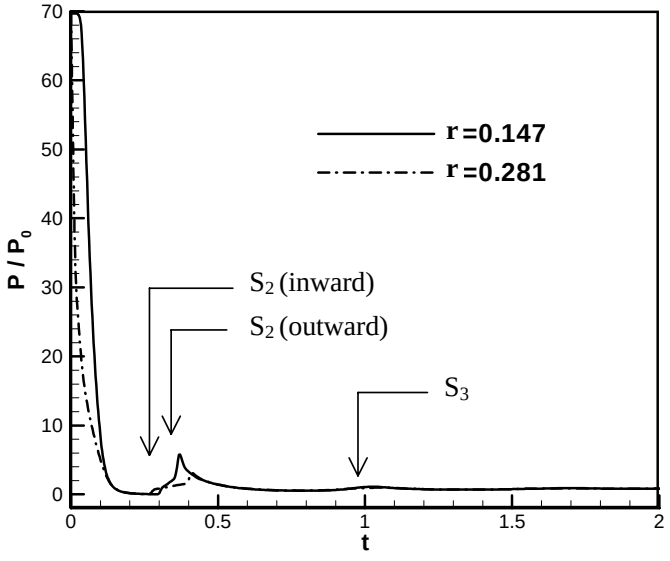

a

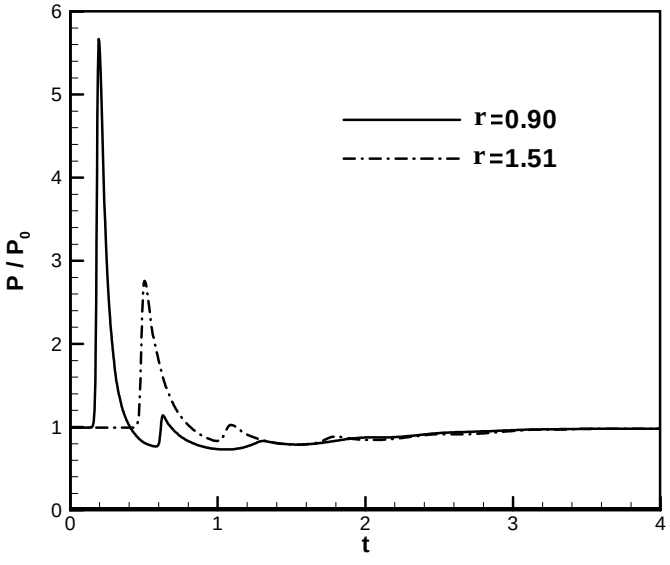

b

Fig. 6. The pressures as function of time at selected locations; **a** inside the bursting sphere, **b** outside the bursting sphere

ward. At $t = 0.31$ the outward-moving secondary shock wave causes one more pressure rise for the dash-line case. In the same vein, at $t = 1.05$, the tertiary weak shock causes one more mild pressure rise. Finally, the pressures at the specified locations resume the atmospheric pressure. At the other positions outside the sphere, $r = 0.9$, 1.51, one can clearly see the overpressure and under-pressure phases on the pressure-time history, as shown in Fig. 6b. The overpressure phase is due to the shock front, and the under-pressure phase is due to the expansion waves following the shock front. Both phases result in two visible sharp peaks on the pressure-time curves.

3.3 Weak spherical blast-wave interaction with a flat plate

To investigate the blast-wave interaction with the flat plate, the viscous effects are taken into account and the compressible Navier-Stokes solver is used. The flat plate is assumed to be adiabatic. The values of flow parameters are chosen to be the same as in Sect. 3.2. The flow is assumed to be turbulent, and the two-layer algebraic turbulence model of Baldwin and Lomax (1978) is employed. The Reynolds number is chosen to be 5×10^7. The flow condition chosen is the same as in Sect. 3.2.

To study the effect of grid number, the Euler solver is first used for numerical simulation. Five grids – 100×150 (grid 1), 125×188 (grid 2), 137×206 (grid 3), 150×225 (grid 4) and 175×263 (grid 5), are chosen. It was found that the improvement on the maximum pressure on the flat plate is 10.4% for changing grid 1 to grid 2, 8% for changing grid 2 to grid 3, 3.3% for changing grid 3 to grid 4, and 0.6% for changing grid 4 to grid 5. Since the improvement of grid refinement from grid 4 and grid 5 is less than 1%, grid 4 is used for subsequent study. Next, we add more grid points in the x-direction (the vertical direction in Fig. 1) in order to take the boundary layer into account for a viscous flow. Therefore, a 180×225 grid is chosen for the laminar-flow calculation, and a 190×225 grid for the turbulent-flow calculation. The smallest x-direction spacing is 0.001 and 0.00015, respectively. It was found that there is a numerical, artificial wave reflection from the top boundary for $t \geq 3$. At this instant, the main shock front is inclined with the top boundary at a small angle and causes a problem of difficult treatment on the non-reflecting boundary condition. To avoid the numerical flaw, the computational domain is further enlarged in the x-direction to a larger domain, $\{(x, y)|0 \leq x \leq 6, 0 \leq y \leq 6\}$, and a 255×225 grid is used for the laminar-flow calculation and 265×225 for the turbulent-flow calculation.

Figure 7 shows the comparison of the pressure contours at $t = 1.8$ and 3 for different flows. One can see that the reflected shocks of the secondary and tertiary shocks, S_2, S_3, in the viscous flow either laminar or turbulent become very weak compared with those for the inviscid flow. The weakening of the reflected shocks is due to the effect of the boundary layer as the flow energy is dissipated. There is a flaw in the numerical simulation, which is the artificial wave reflection from the upper boundary. To avoid the artificial reflected wave, one can enlarge the computational domain by moving up the upper boundary or improve the non-reflecting boundary condition imposed there.

The transition in the type of shock wave reflection is also interesting. In order to observe the transition, a rule is made to determine a Mach reflection. We plotted the density distributions at the altitude of $x = 0.104$ above the flat plate for viscous flow and at $x = 0.105$ for inviscid flow at various instants. We found that the formation of a Mach reflection corresponds to the occurrence of a wiggle in the density distribution. It was found that the interaction of the blast wave with the flat plate produces only a $RR \Rightarrow MR$ transition. The transition occurred ap-

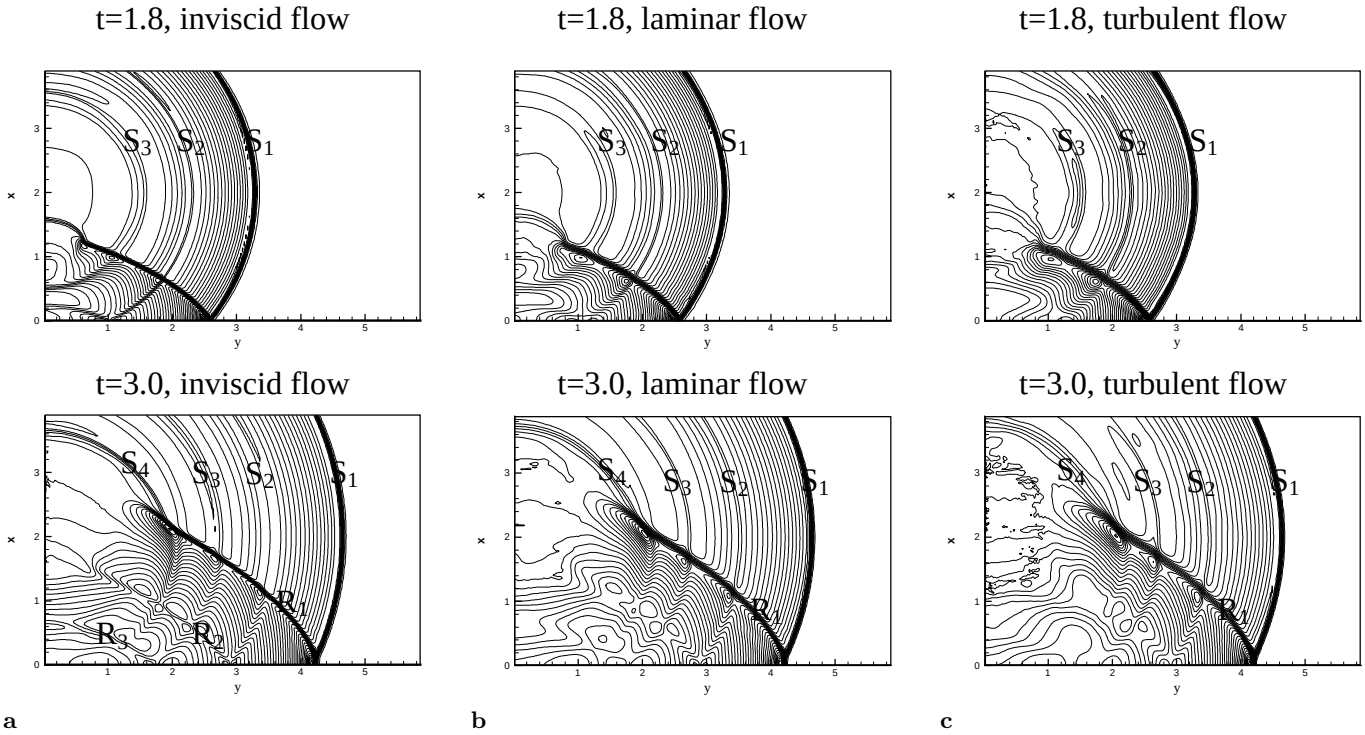

Fig. 7. A comparison of the pressure contours for the interaction of a blast wave with the flat plate at $t = 1.8$ and 3.0, $P_1/P_0 = 70$, $HOB = 2.0$, **a** inviscid flow, **b** laminar flow, **c** turbulent flow

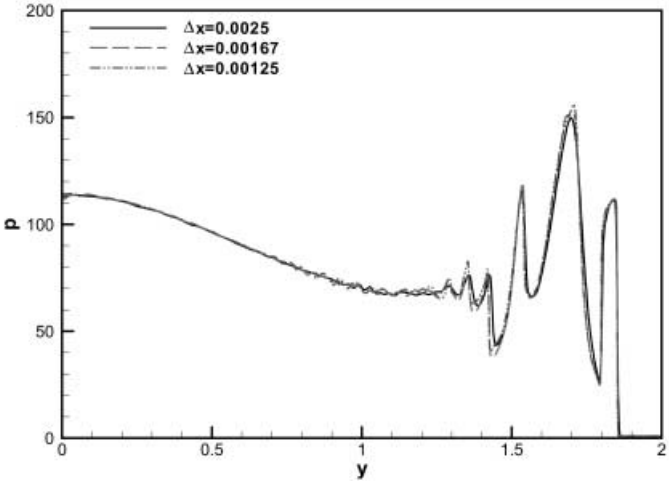

Fig. 8. Comparison of the wall pressures on different grids at $t = 0.13$

proximately at $y = 1.55$–1.67 for the inviscid- and viscous-flow calculations, and $y = 1.66$–1.76 for the turbulent-flow calculation. That means that a delayed transition phenomenon occurs in a turbulent flow.

3.4 Strong blast-wave interaction with a flat plate

From Sect. 3.3 one can see that, by using an inviscid-flow model, the basic flow structure is not significantly different from that obtained by the viscous (laminar or turbulent) model. So, in this case of strong blast wave, we only consider the inviscid-flow model for saving computation time. We chose the initial pressure ratio of $p_1/p_0 = 400$, $R_0 = 1$, and $HOB = 1$, for producing a strong blast wave. Obviously, real gas effects take place in this case. The computational domain is chosen to be $\{(x, y)|0 \le x \le 1, 0 \le y \le 2\}$. The effect of grid number was also studied. Three different uniform grids with grid points of 400×800 (grid 1), 600×1200 (grid 2), 800×1600 (grid 3) were chosen. We have checked the effect of grid number on the (dimensionless) wall pressures at different instants, $t = 0.066$, 0.9 and 0.13. It is clearly shown that the wall pressure and the locations of shocks developed on the flat plate are almost independent of grid number. The comparison of the predicted wall pressures on different grids at $t = 0.13$ is shown in Fig. 8. Other two cases are omitted due to space limitation. From Fig. 8, one can see that grid 1 is fine enough to predict reasonably accurate result.

Figure 9 shows the flow structures of isopycnics and pressures at different instants for grid 2. At $t = 0.066$, the incident shock (I) is reflected from the flat plate with the type of regular reflection, and is near the transition instant of $RR \Rightarrow DMR$. Near the reflection point, the incident shock (blast) and the reflected shock (R) have an inclination angle of 49 deg and 37 deg respectively. By comparing the pressure and density contours, we found that there is a contact surface (CS) accompanying the blast wave. The reflected shock is curved upward to intercept and penetrate the contact surface (CS), resulting in a triple point where a Mach stem emitted toward the contact surface. There is a very high-pressure region that occurs below the reflected wave. In this region, the pres-

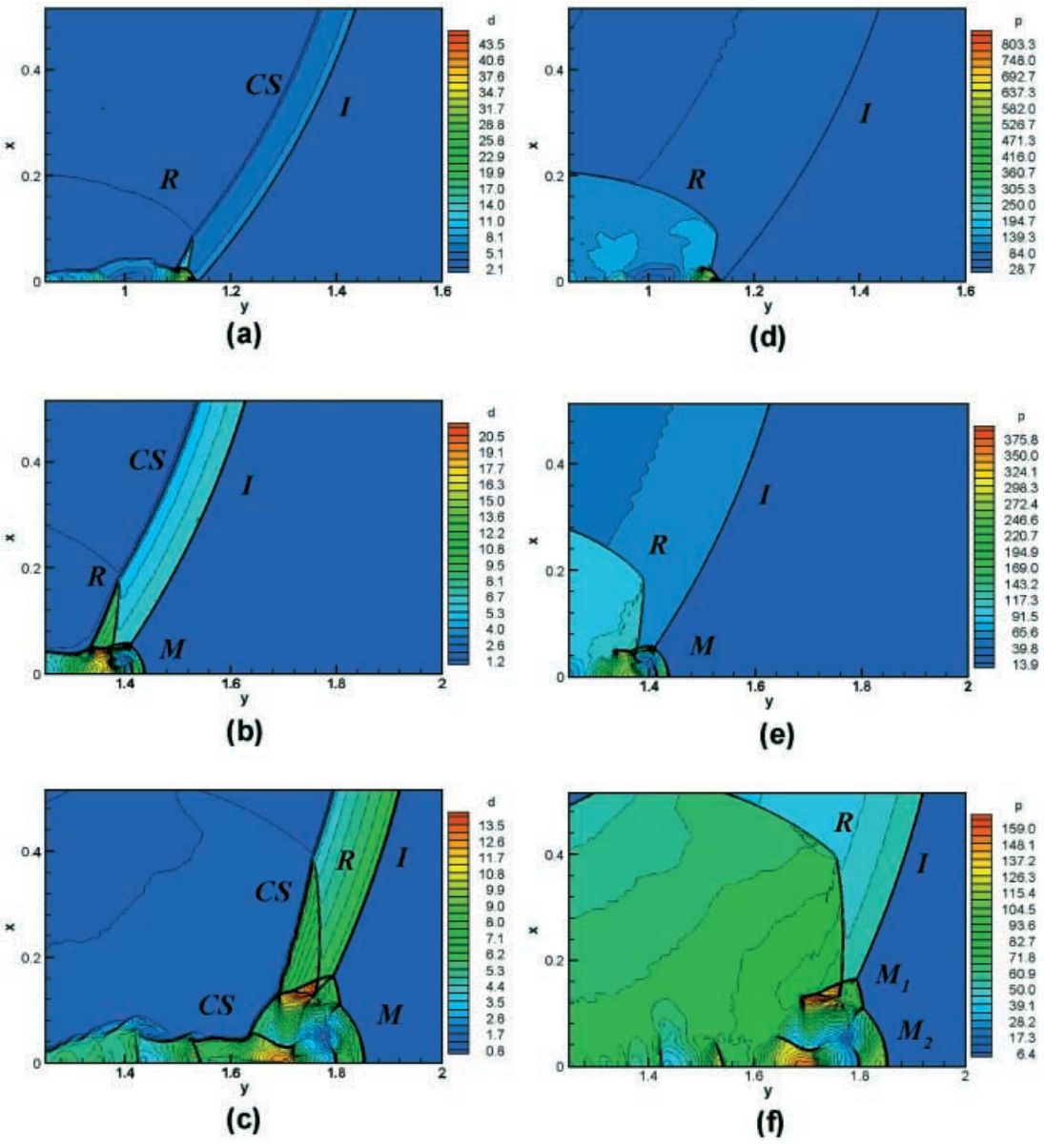

Fig. 9. The computed flow fields of (**a**–**c**) isopycnic and (**d**–**f**) pressure for the problem of a strong blast wave interacting with a flat plate at different instants. **a, d** $t = 0.066$; **b, e** $t = 0.09$; **c, f** $t = 0.13$

sure is the highest in the whole flow field. At $t = 0.09$, the type of wave reflection has evolved into a double Mach reflection with a curved Mach stem (M) associated with the incident shock wave. There is a high pressure developed in the region, $\{(x, y)|1.33 < x < 1.37, 0 < y < 0.046\}$. As mentioned before, the highest-pressure region did not occur behind the curved Mach stem. At $t = 0.13$, the curved Mach stem (M) has developed into two parts. One is a straight part (M_1); the other is a curved part (M_2). There are also four nearly normal shocks developed on the flat plate, causing three local high-pressure regions (orange color or yellow color region) behind each normal shock. There are other high-pressure regions near the reflected shock waves, denoted by the orange color. We believed that these high dynamic pressure regions constitute an over-turning effect for tactical equipments experiencing a very high explosion in addition to the crushing effect of the incident blast wave. Moreover, we plotted the velocity field behind the curved Mach stem, and did not find any rotational flow. Our result is quite different from that of Colella et al. (1986). They found a rotational flow behind the curved Mach stem, which was attributed to improper grid zoning and numerical viscosity.

4 Conclusions

A high-resolution Euler/Navier-Stokes solver with a real-gas model has been developed and used to investigate the propagation of a spherical blast wave in the free field and the reflection phenomenon of the blast wave when interacting with the flat plate. The solver has been validated to

be reasonably accurate on several test problems. For the problem of blast-wave propagation in the free field, it is found that three outward-moving weaker shock waves are developed behind the primary shock wave and a contact surface is formed at $r = 0.99$.

For the problem of the weak blast-wave interaction with the flat plate, a complicated flow structure of the shock-shock interactions in addition to the basic flow structure for the blast-wave propagation in a free field is presented. Moreover, it is found that there is a delayed transition phenomenon of $RR \Rightarrow MR$ in a turbulent flow compared with that for an inviscid flow or a laminar flow. For the problem of the strong blast-wave interaction with the flat plate, a complicated flow structure associated with the transition from regular reflection to double Mach reflection is investigated. It is found that near the flat plate there are at least three local high-pressure regions behind the curved Mach stem, resulting in an over-turning effect in addition to the crushing effect in very high explosions.

Acknowledgements. The support for the work under the National Science Council contract, NSC 89-2612-E-006-018, is gratefully acknowledged. The authors are also indebted to Professor J. M. Dewey and reviewers for their valuable comments.

References

Baldwin B, Lomax H (1978) Thin-layer approximation and algebraic model for separated turbulent flows. AIAA paper 78-257

Brode HL (1955) Numerical solutions of spherical blast waves. J. App. Phys. 26:766–775

Brode HL (1959) Blast wave from a spherical charge. Phys. of Fluids 2:217–229

Colella P, Ferguson, RE, Glass HM, Kuhl AL (1986) Mach reflection from an HE-driven blast wave. Procedding of 10th ICDERES, Berkeley, California, Aug. 4-9 1985, AIAA Inc., New York, pp. 388–421

Deschambault RL and Glass II (1983) An update on nonreflecting oblique shock-wave reflection. J. Fluid Mech. 131:27–57

Dewey JM (1971) The properties of a blast wave obtained from an analysis of the particle trajectories. Proc. R. Soc. Lond. A. 324:275–299

Dewey JM, McMillin DJ (1981) An analysis of the particle trajectories in spherical blast waves reflected from real and ideal surfaces. Can. J. Phys. 59:1380–1390

Dixon-Hiester LA, Reisler RE, Keefer JH, Ethridge NH (1990) Shock enhancement at transition from regular to Mach reflection. Proc. of the 17th Int. Symp. on Shock Waves and Shock Tubes, July 17–21, Bethlehem, PA, 1989, American Institute of Physics, New York, pp. 204–209

Grossman B, Walters RW (1989) Analysis of flux-split algorithms for Euler's equations with real gases. AIAA J. 27:524–531

Hisley, DM (1990) BLAST2D computations of the reflection of planar shocks from wedge surfaces with comparison to SHARC and STEALTH results. Report No. BRL-TR-3147, NTIS No. AD-A227 261/5/HDM

Hoffmann, KA, Chiang, ST (1993) Computational fluid dynamics for engineers. Engineering Education System^{TM}, Wichita, Kansas, 2:69

Hu TCJ, Glass II (1986) Blast wave reflection trajectories from a height of burst. AIAA J. 24:607–610

Jiang GS, Shu C-W (1996) Efficient implementation of weighted ENO schemes. J. Comp. Phys. 126:202–228

Jiang Z, Takayama K, Moosad KPB, Onodera O, Sun M (1998) Numerical and experimental study of a micro-blast wave generated by pulsed-laser beam focusing. Shock Waves 8:337–349

Srinivasan S, Tannehill JC (1987) Simplified curve fits for the thermodynamic properties of equilibrium air. NASA CR-178411

Srinivasan S, Tannehill JC, Weilmuenster KJ (1987) Simplified curve fits for the transport properties of equilibrium air. NASA RP-1181

Takayama K, Sekiguchi H (1981) Formation and diffraction of spherical shock waves in a shock tube. Rep. Inst. High Speed Mech. 43:89–119

Thompson KW (1987) Time dependent boundary conditions for hyperbolic systems. J. Comp. Phys. 68:1–24

Vanderstraeten B, Lefebvre M, Berghmans J (1996) A simple blast wave model for bursting spheres based on numerical simulation. J. Hazardous Materials 46:145–157

Wang JS (2000) Numerical simulation of spherical blast wave propagation and reflection. Master Thesis, Department of Aeronautics and Astronautics, National Cheng Kung University, Tainan, Taiwan, Republic of China